https://doi.org/10.5194/amt-2020-291
Preprint. Discussion started: 29 July 2020

Atmospheric Measurement Techniques Discussions

Combined use of Mie-Raman and fluorescence lidar observations for improving aerosol characterization: feasibility experiment

Igor Veselovskii[1], Qiaoyun Hu[2], Philippe Goloub[2], Thierry Podvin[2], Mikhail Korenskiy[1], Olivier Pujol[2], Oleg Dubovik[2], Anton Lopatin[3]

[1]*General Physics Institute, Vavilova st., 38, Moscow, 119991, Russia.*

[2]*Univ. Lille, CNRS, UMR 8518 - LOA - Laboratoire d'Optique Atmosphérique, Lille F-59000, France*

[3]*GRASP-SAS, Villeneuve d'Ascq, France*

Abstract

To study the feasibility of a fluorescence lidar for aerosol characterization, the fluorescence channel is added to LILAS - multiwavelength Mie-Raman lidar of Lille University, France. A part of fluorescence spectrum is selected by the interference filter of 44 nm bandwidth centered at 466 nm. Such an approach has demonstrated high sensitivity, allowing to detect fluorescence signal from weak aerosol layers (backscattering coefficient at 1064 nm is below 0.02 $Mm^{-1}sr^{-1}$) up to a height of 5000 m. Simultaneous detection of nitrogen Raman and fluorescence backscatters allows to quantify the fluorescence backscattering coefficient. Observations were performed during November 2019 – February 2020 period. The fluorescence capacity (ratio of fluorescence to elastic backscattering coefficients) varied in a wide range, being the highest for the smoke and the lowest for the dust particles. The fluorescence capacity depends as well strongly on the relative humidity, because the water uptake at the condition of high RH increases the elastic backscattering, without significant modification of the fluorescence. Thus, simultaneous measurements of Mie-Raman and fluorescence lidars open opportunity for the study of the particle hygroscopic growth. The fluorescence technique can be used also for monitoring the aerosol inside the cloud layers. The results presented demonstrate, that aerosol and cloud particles can be mixed both externally and internally. When the cloud is formed at the top or inside the aerosol layer (such scenario can be probably considered as internal mixing) we observed significant (up to factor 5) increase of fluorescence backscattering. Among possible mechanisms of such enhancement we can assume modification of the scattering phase function of the particles embedded in the water microspheres and the lens effect due to the water shell presence.

1. Introduction

https://doi.org/10.5194/amt-2020-291
Preprint. Discussion started: 29 July 2020


Atmospheric Measurement Techniques Discussions

The aerosol – cloud interaction is one of the key factors influencing the Earth radiation balance and, for its realistic modeling, knowledge of aerosol properties both outside and within the cloud layer are needed. The multiwavelength Mie-Raman and HSRL lidars, measuring aerosol backscattering and extinction coefficients at multiple wavelengths, are widely used for remote characterization of aerosol properties (Burton et al., 2012). However, although useful for studying aerosol, the amount of information contained in these measurements remains limited (Burton et al., 2016; Alexandrov and Mishchenko, 2017). In addition, such lidars are not able to detect and characterize aerosol inside a cloud layer, because aerosol scattering is masked by the strong cloud particles scattering. To improve the lidar capability for aerosol characterization, additional channels, measuring the laser induced fluorescence, can be used. Moreover, the fluorescence provides unique opportunity to detect (and characterize) aerosol particles within cloud layer, at least near the cloud base, thus allowing to investigate the aerosol – cloud coexistence.

Fluorescence spectroscopy is a highly sensitive technique, widely used for the in-situ monitoring of atmospheric organic particles (Pan et al., 2007, 2015; Miyakawa et al., 2015; Huffman et al., 2019). The synergy of fluorimetry and lidar technology provides an opportunity to perform such monitoring remotely (Immler et al., 2005; Rao et al., 2018; Saito et al., 2018). Numerous types of atmospheric aerosols, such as biological particles, biomass burning and even dust particles are fluorescent, being excited by UV radiation. When the excitation wavelength is 355 nm, the main part of emission spectra is usually contained within the 400–650 nm range (Pan et al., 2015). The fluorescence spectrum varies with the aerosol types/composition, making therefore possible their identification.

The recent interest in fluorescence lidars was stimulated also by the progress in the development of the multianode photomultipliers allowing, in combination with spectrometer, simultaneous detection of lidar signal in 32 spectral bins (Sugimoto et al., 2012; Reichardt et al., 2014, 2017; Saito et al., 2018). Such multichannel detection has the obvious advantage to analyze the whole spectrum, allowing the aerosol identification. However, sensitivity of such lidar spectrometers is low when compared to the standard technique based on selection of fluorescence spectrum intervals with interference filters (Immler et al, 2005; Rao et al., 2018; Li et al., 2019). Such an approach, in addition to being more sensitive, allows more affordable modification of a multiwavelength Mie-Raman lidar by adding one or more fluorescence channels.

To obtain the highest sensitivity, it is mandatory to acquire the fluorescence in a wide spectral range which, however, makes the data analysis more complicated, because variation of aerosol and molecular transmission within the detection spectral range has to be accounted for.

https://doi.org/10.5194/amt-2020-291
Preprint. Discussion started: 29 July 2020


Atmospheric Measurement Techniques Discussions

In addition, in Mie-Raman multi-wavelength lidars one should avoid the spectral intervals affected by elastic scattering and corresponding strong Raman lines. In this work, we present the results of a feasibility experiment and evaluate the sensitivity of a single-channel fluorescence lidar to different aerosol types. We focus in this study also on the possibility to monitor the aerosol fluorescence within a cloud layer. However, to obtain quantitative measurements of aerosol content within a cloud layer, several factors should be considered.

First of all, external/internal mixtures of aerosol particles with water droplet should be distinguished. In case of external mixture, the fluorescence signal can be used directly for the estimation of the particle concentration, if the particle type and corresponding fluorescence cross section are known. For internal mixture (aerosol particle is inside the water droplet) the fluorescence backscattering can be enhanced due to modification of the scattering phase function of the particles embedded in the water microspheres (Kerker and Druger, 1979; Veselovskii et al., 2002a). For insoluble particle, the presence of the water shell can lead also to an additional increase of the fluorescence, due to the water droplet lens effect. Similar effect is well known for the soot particles covered by non-absorbing shell (Schnaiter, 2005).

In our paper we present the results of fluorescence measurements performed at *Laboratoire d'Optique Atmosphérique* (LOA) during November 2019 – February 2020 period. During that period, the aerosol load was very low, so we were not able to determine the particle properties from multiwavelength observations. The objective was then to estimate the efficiency /added value of the fluorescence channel. We therefore mainly focus on analysis of efficiency of fluorescence lidar monitoring of different types of aerosol and on detection of aerosol particles inside low level cloud layer.

2. Experimental setup and data analysis

The measurements were performed using the LILAS - multiwavelength Mie-Raman lidar, based on a tripled Nd:YAG laser with a 20 Hz repetition rate and pulse energy of 70 mJ at 355 nm. The backscattered light is collected by a 40 cm aperture Newtonian telescope. The system is designed for simultaneous detection of elastic and Raman backscatters, allowing the so called $3\beta+2\alpha+3\delta$ data configuration, including three particle backscattering (β), two extinction (α) coefficients along with three depolarization ratios (δ). Description of the system can be found in recent publication of Hu et al., 2019. The aerosol extinction and backscattering coefficients at 355 and 532 nm were calculated from Mie-Raman observations (Ansmann et al., 1992) while β_{1064} was derived by the Klett method (Klett, 1985).

For the experiment described, the system was modified: water vapor 408 nm Raman filter was replaced by a fluorescence one. Corresponding optical scheme together with transmission

https://doi.org/10.5194/amt-2020-291
Preprint. Discussion started: 29 July 2020

Atmospheric Measurement Techniques Discussions

curve of the interference filter in the fluorescence channel are shown in Fig.1. The nitrogen Raman and fluorescence optical signals are separated by a dichroic mirror: more than 98% of 387 nm radiation is reflected and more than 95% of fluorescence signal is transmitted. For both nitrogen Raman and fluorescence channels, the R9880U-01 PMTs were used. A part of the wideband fluorescence signal was selected by an Alluxa interference filter centered at 466 nm with 44 nm bandwidth. The filter transmission, at maximum, exceeds 98%. The operational band was chosen outside of the overtones of O_2 and N_2 vibrational Raman lines. In addition, the transmission of the selected fluorescence filter band matches the maxima of fluorescence of many organic molecules (Saito et al., 2018; Reichardt et al., 2017). Filter provides OD6 suppression outside the transmission band. To increase the suppression, two identical interference filters were used in tandem. For additional rejection of elastic scattering at 355 nm and 532 nm the two-band notch filter was used. With such design, we estimate that the total suppression of elastic scattering in the fluorescence channel is above OD14. In this paper, observations were carried out during night-time only.

In an elastic channel, the backscattered radiative power P_L, at distance z is described by the lidar equation

$$P_L = O(z)\frac{1}{z^2}C_L(\beta_L^a+\beta_L^m)\exp\left\{-2\int_0^z(\alpha_L^a+\alpha_L^m)dz'\right\} = O(z)\frac{1}{z^2}C_L(\beta_L^a+\beta_L^m)T_L^2 \quad (1)$$

Here O(z) is the geometrical overlap factor, which is assumed to be the same for elastic, Raman and fluorescence channels. C_L is the range independent constant, including efficiency of detection channel. T_L is one-way transmission, describing light losses on the way from the lidar to distance z at laser wavelength λ_L. Backscattering and extinction coefficients contain aerosol and molecular contributions: $\beta_L^a+\beta_L^m$ and $\alpha_L^a+\alpha_L^m$, where the superscripts “a” and “m” indicate aerosol and molecular scattering, respectively.

In a Raman channel, the backscatter radiative power, P_R , can be rewritten as:

$$P_R = O(z)\frac{1}{z^2}C_R\beta_R\exp\left\{-\int_0^z(\alpha_L^a+\alpha_R^a+\alpha_L^m+\alpha_R^m)dz'\right\} = O(z)\frac{1}{z^2}C_R\beta_R T_L T_R \quad (2)$$

Here T_R is the atmospheric transmission at Raman wavelength λ_R. Raman backscattering coefficient is:

$$\beta_R = N_R\sigma_R, \quad (3)$$

where N_R is the number of Raman scatters (per unit of volume) and σ_R is the Raman differential scattering cross section in the backward direction. To account for spectral dependence of aerosol extinction, the Angstrom exponent γ is used:

https://doi.org/10.5194/amt-2020-291
Preprint. Discussion started: 29 July 2020

Atmospheric Measurement Techniques Discussions

$$\frac{\alpha_L^a}{\alpha_R^a} = \left(\frac{\lambda_R}{\lambda_L}\right)^{\gamma} \quad (4)$$

The aerosol backscattering and extinction coefficients can be computed from Mie – Raman lidar observations using equations (1-4), as shown by Ansmann et al. (1992).

In the case of the fluorescence, the emitted wavelengths are spread over wide spectral range, so the spectral dependence of aerosol and molecular extinction coefficients, inside the fluorescence band, should be considered. Moreover, the spectral differential fluorescence cross section $\frac{d\sigma_F}{d\lambda}(\lambda, r)$ depends on particle size (Hill, et al., 2015), so the particle number size distribution $\frac{dN(r)}{dr}$, which is the number of particles with radii between *r* and *r*+*dr* per unit of volume, has to be considered. The radiative power in the fluorescence channel within the spectral interval $[\lambda_{min},\lambda_{max}]$ is:

$$P_F = O(z)\frac{1}{z^2}T_L \int_{\lambda_{min}}^{\lambda_{max}} \int_{r_{min}}^{r_{max}} C_F(\lambda) \times \frac{dN(r)}{dr} \times \frac{d\sigma_F}{d\lambda}(\lambda, r) \times \exp\left\{-\int_0^z [\alpha^a(\lambda, z') + \alpha^m(\lambda, z')]dz'\right\} dr d\lambda \quad (5)$$

The spectral dependence of $C_F(\lambda)$ is determined mainly by the transmission of the interference filter in the fluorescence channel. If the filter spectral width $\lambda_{max} - \lambda_{min}$ is not very high, the procedure of data analysis can be simplified. The atmospheric transmission for fluorescence signal

$$T_F(\lambda) = \exp\left\{-\int_0^z [\alpha^a(\lambda, z') + \alpha^m(\lambda, z')]dz'\right\} \quad (6)$$

can be taken at wavelength λ_F, corresponding to the center of the filter transmission band $T_F(\lambda) = T_F(\lambda_F) \equiv T_F$. The filter transmission used (Fig.1) is close to rectangular and sensitivity of the PMT used doesn't vary significantly within $[\lambda_{min}, \lambda_{max}]$ interval, which means the calibration constant C_F can be considered as spectrally independent. Expression (5) can be rewritten, by introducing the fluorescence backscattering coefficient β_F:

$$\int_{\lambda_{min}}^{\lambda_{max}} \int_{r_{min}}^{r_{max}} \frac{dN(r)}{dr} \times \frac{d\sigma_F}{d\lambda}(\lambda, r) dr d\lambda = \int_{r_{min}}^{r_{max}} \frac{dN(r)}{dr} \times \sigma_F(r) dr = \beta_F \quad (7)$$

Here $\sigma_F(r) = \int_{\lambda_{min}}^{\lambda_{max}} \frac{d\sigma_F}{d\lambda}(\lambda, r) d\lambda$ is the effective fluorescence differential cross section, integrated over spectral interval $[\lambda_{min}, \lambda_{max}]$. The use of β_F allows to rewrite equation (5) for the power of the fluorescence backscattering similarly to the Raman one.

https://doi.org/10.5194/amt-2020-291
Preprint. Discussion started: 29 July 2020


Atmospheric Measurement Techniques Discussions

$$P_F = O(z)\frac{1}{z^2}C_F\beta_F T_F T_L \quad (8)$$

The fluorescence backscattering coefficient, β_F, can be obtained from the ratio of equations (8) and (2) for fluorescence and Raman backscatters:

$$\beta_F = \frac{C_R}{C_F}\frac{P_F}{P_R}N_R\sigma_R\frac{T_R}{T_F} \quad (9)$$

The ratio of atmospheric transmissions at λ_R and λ_F wavelengths (T_R/T_F) can be calculated the same way as for water vapor measurements (Ansmann et al., 1992; Whiteman et al., 2006). In our study, for the nitrogen molecule we used Raman scattering cross section at 355 nm $\sigma_R=2.1*10^{-30}$ cm^2 (Burris et al., 1992), but, to obtain absolute values of β_F, C_R/C_F ratio must be determined. This ratio can be found from calibration, performed by using a lamp with known spectrum, as it has been done for the Raman water vapor lidars (Venable et al., 2011). At current stage, for β_F estimations, we assume that sensitivities of PMTs in both channels are similar (switching of PMTs between N_2-Raman and fluorescence channels didn't change results noticeably), thus only difference in transmission of interference filters was considered. In all results presented below C_R/C_F=0.7 value was used for calculations.

To characterize the efficiency of the fluorescence respect to elastic scattering, it is convenient to consider also the particle fluorescence capacity, $G_F = \frac{\beta_F}{\beta_L}$, which is the ratio of fluorescence and aerosol elastic backscattering coefficients (Reichardt et al., 2017). Here and below, for simplicity, we will use notation $\beta^a \equiv \beta$. The aerosol loading in the atmosphere during the experiment was very low and, in order to decrease the interference of the Raleigh scattering, the backscatter at 1064 nm was mainly used for aerosol characterization, while for the cloud layers the backscattering coefficients at 355 and 532 nm were used as well.

Multiwavelengtn Mie-Raman lidar measurements allow estimation of the particle number density $N = \int_{r_{min}}^{r_{max}} \frac{dN(r)}{dr}dr$ as well as their total volume V (Müller et al., 1999; Veselovskii et al., 2002b), thus a mean fluorescence cross section per a single particle can be estimated as $\sigma_F^N = \frac{\beta_F}{N}$. Assuming, that in the simplest case, a fluorescence backscattering coefficient is proportional to the particle volume, we can estimate the fluorescence cross section per a unit particle volume as $\sigma_F^V = \frac{\beta_F}{V}$. Thus, synergy of Mie-Raman and fluorescence lidar measurements should allow remote characterization of the particle fluorescent properties.

https://doi.org/10.5194/amt-2020-291
Preprint. Discussion started: 29 July 2020

Atmospheric Measurement Techniques Discussions

3. Observation results.

3.1. Fluorescence of aerosol layers.

The measurements reported were performed during November 2019 – February 2020 period at the Lille Atmospheric Observation Platform (https://www-loa.univ-lille1.fr/observations/plateformes.html?p=apropos) hosted by Laboratoire d'Optique Atmospherique, University of Lille, Hauts-de-France region. Two examples of measurement are presented in Fig.2 and are showing height–temporal distributions of the range corrected lidar signal (RCS) at 1064 nm, of volume depolarization ratio, δ_{1064}, and of fluorescence backscattering coefficient, β_F, for the nights 29-30th November 2019 and 6-7th February 2020.

During the first night (left column in Fig. 2), aerosol layer is localized mainly below 2000 m. Though the aerosol loading is low (β_{1064}<0.01 $Mm^{-1}sr^{-1}$) above 2000 m, it is well revealed by the enhanced depolarization ratio and the enhanced fluorescence backscattering coefficient. During the second night of observation (right column in Fig.2), a detached/isolated layer is observed at approximately 3000 m. This layer is characterized by high depolarization ratio (the particle depolarization ratio at 1064 nm in the center of the layer exceeds 15%), indicating to the presence of dust. An explanation of the observed increase of fluorescence signal could be mixing of mineral dust particles with organic materials (Sugimoto et al., 2012; Miyakawa et al., 2015) and local aerosol during transportation.

The time averaged profiles (β_{1064}, β_F, G_F) for these two nights, as well as for 16th January episode are shown in Fig.3. Backscattering coefficient β_{1064} was calculated by Klett method, assuming a lidar ratio S=50 sr. Due to low aerosol extinction value, the results are not sensitive to the choice of S. The closest available radiosonde data are from the Herstmonceux (UK) and Essen (Belgium) stations, located 160 km and 120 km away from the observation site respectively. Data from both stations show that on the night 29-30 November 2019 the relative humidity (RH) was about 70% at 1000 m and dropped below 20% above 2000 m. Pure water is not fluorescing, so the water uptake by the particle, in the condition of high relative humidity (RH), is expected to yield an increase of elastic scattering without significant effect on the fluorescence emission. The aerosol backscattering β_{1064} on 29-30th November (Fig.3a) is 0.4 $Mm^{-1}sr^{-1}$ at 1000 m and decreases by a factor 40 at 1900 m, while β_F within this height range changes less than twice. This is supporting the assumption that the observed variation of aerosol backscattering in the PBL is mainly due to the change of the particle water fraction. The water uptake at low altitudes agrees with low values of the observed particle depolarization ratio δ^p_{1064}, which is below 0.5% at 1000 m. Within weak aerosol layer at the range 2500 – 4000 m, the particle depolarization δ^p_{1064} is about 5% and we observe the increase of fluorescence capacity G_F,

https://doi.org/10.5194/amt-2020-291
Preprint. Discussion started: 29 July 2020

Atmospheric Measurement Techniques Discussions

with respect to the layer below 2000 m, up to $2.5*10^{-4}$. This increase of G_F in the 2500 – 4000 m layer can be due to the presence of another particles type, for example, biomass burning. From this episode, one can conclude that fluorescence backscattering, though being almost 4 orders lower than elastic one, can be reliably detected with our current lidar configuration.

On January 16th (Fig.3b), atmospheric RH also decreases with height, from about 80% at 1000 m to less than 20% above 2000 m, leading to an increase of G_F for more than one order of magnitude. Such variation of G_F within the PBL is probably also related to the particle water uptake, just like in Fig.3a. Aerosol backscattering increases above 3000 m and reaches its maximum value at 5000 m. Within 3000 m – 5500 m range, fluorescence capacity was about $2.5*10^{-4}$, which is higher than in the PBL.

On February 6-7th the aerosol loading in the PBL is very low (β_{1064}<0.003 $Mm^{-1}sr^{-1}$ at 1000 m) and RH from radiosonde at Herstmonceux is below 40% in the height range considered. At 3000 m, a dust layer is observed (Fig.3c). In the middle of this layer, fluorescence capacity is about $0.6*10^{-4}$ which is about factor 4 lower than in the elevated layers in Fig.3a,b. Still, significant value of G_F can indicate the presence of organic materials in the dust layer (Sugimoto et al., 2012).

As discussed in section 2, lidar measurements provide an opportunity to estimate the particle fluorescence cross section. For this, we need to know the particle number N and volume V density in the aerosol layer, which, in principle, can be determined from the multiwavelength lidar observations (Muller et al., 1999; Veselovskii et al., 2002b). In our case, however, due to very low aerosol loading the extinction coefficients could not be determined. Still, the rough estimations of the particle parameters can be done using the predefined aerosol model driven by only a few parameters. In our study we use a simplified approach, modeling aerosol as an external mixture of several aerosol components with predetermined properties. The definition of aerosol components is based on global multiyear AERONET observations (Dubovik et al., 2002) with some modifications. All aerosol types are described by a bimodal particle size distribution (PSD)

$$\frac{dV}{d\ln r} = \sum_{i=f,c} \frac{C_{V,i}}{\sqrt{2\pi}\sigma_i} \exp\left[-\frac{(\ln r - \ln r_{V,i})^2}{2\sigma_i^2} \right] \quad (10)$$

where $C_{V,i}$ denotes the particle volume concentration, $r_{V,i}$ is the median radius, and σ_i is the standard deviation. Subscripts f and c correspond to the fine and coarse mode respectively. The parameters of the number size distribution $\frac{dN}{d\ln r}$ can be obtained from (10) using the expressions from Horvath et al. (1990). Table 1 shows the model parameters for three aerosol

https://doi.org/10.5194/amt-2020-291
Preprint. Discussion started: 29 July 2020

Atmospheric Measurement Techniques Discussions

types: biomass burning (BB), urban (UR) and dust (DU). From this model, the aerosol backscattering and extinction coefficients can be calculated at any wavelength. As mentioned above, due to low aerosol loading, we use only backscattering coefficient at 1064 nm, so Table 1 presents $\beta_{1064}^{N} = \frac{\beta_{1064}}{\int_{r_{min}}^{r_{max}} \frac{dN(r)}{dr} dr}$ - mean backscattering coefficient for a single particle (N=1), together with corresponding complex refractive index (CRI) used in computations. Calculations were performed in assumptions of spherical particles for BB and UR and for the randomly oriented spheroids for dust (Dubovik, et al., 2006). The volume $V^{N=1}$ in the Table 1 is also given for N=1 (so can be considered as a single particle average volume). Thus, if the aerosol type is known, comparing of computed $\beta_{1064}^{N=1}$ from Table 1 with observed values β_{1064}, yields the number and volume particle densities as $N = \frac{\beta_{1064}}{\beta_{1064}^{N=1}}$ and $V = N \times V^{N=1}$.

Table 2 summarizes for the three nights from Fig.3, the fluorescence cross sections per a single particle, $\sigma_F^N = \frac{\beta_F}{N}$, and per unit volume, $\sigma_F^V = \frac{\beta_F}{V}$. Values are provided for the altitudes corresponding to the maximum of fluorescence backscattering β_F in elevated layers, where the relative humidity (RH) should be low and hygroscopic effect reduced. Particles are assumed to be of biomass burning origin for November 30th and January 16th, and from dust origin for February 6-7th. We should remind, however, that our estimations of N (and so σ_F^N) are rough, since they depend on the assumed aerosol type. The particle volume, V, is however a more reliable parameter. For example, if the UR aerosol type is considered, rather than the BB one, the particle number density, N, for November 30th becomes N=21cm^{-3} (instead 63 cm^{-3} for BB) while the total volume remains rather constant (V=0.34 μm^3·cm^{-3} instead of 0.37 μm^{3}cm^{-3}). Thus, presentation of cross section per a unit of volume σ_F^V appears more trustable. The fluorescence cross sections σ_F^V for November 30th and January 16th are very close, but for the dust layer (February 6-7th, 2020), the cross section is about a factor 4 lower. From the data presented it is also possible to estimate the spectral differential cross section, $\frac{\sigma_F^V}{\Delta\lambda}$, where $\Delta\lambda$ is the width of the filter transmission band.

It is rather difficult to validate our values of the fluorescence differential cross section. We nevertheless compare them to in situ ground-based fluorescence measurements. Such reference data are available mainly for biological particles (e.g. Pan, 2015). For biological particles, the

https://doi.org/10.5194/amt-2020-291
Preprint. Discussion started: 29 July 2020


Atmospheric Measurement Techniques Discussions

highest $\frac{d\sigma_F}{d\lambda}$ value, for a single particle with diameter 1.2 μm – 3.0 μm varies in the range (1-100)*10^{-15} $cm^2sr^{-1}nm^{-1}$ when stimulating radiation at 365 nm is used (Pan, 2015). Thus, our estimated values look reasonable, keeping in mind that the fluorescence cross section of the biological particles is higher than that of smoke.

3.2. Fluorescence of aerosol particles within cloud layers

One of the attractive features of the fluorescence technique is the possibility to detect aerosol and derive its content within the cloud layer. However, aerosol and cloud particles can be mixed externally or internally. In the first case, the estimation of the dry particle volume is more or less straightforward, using the fluorescence cross sections obtained from the measurements in the aerosol layers. For the internal mixing, aerosols are located inside the water droplet in solid or dissolved state. It is known, that the fluorescence of microspheres can be increased in the backward direction by factor ~2, comparing to fluorescence of a bulk material, due to modification of the scattering phase function (Kerker et al., 1979; Veselovskii et al., 2002a). Moreover, a fluorescence cross section of solid substance may differ from dissolved one. All this complicates the quantification of the measurements for the case of internal mixing.

The results from November 13th and 18th, representing an **external** mixture case of aerosol and clouds particles, are shown in Fig. 4. The backscattering coefficients are given at 532 nm, because in the cloud layers the detector in 1064 nm channel was sometimes saturated. On November 13th, we observe a strong oscillation of $\beta_{532,}$ due to the contribution of the cloud layers within 1000 m – 3000 m. The increase of β_{532}, however, does not lead to significant enhancement of the fluorescence backscattering β_F in the range of 1000—3000 m.

On 18th November, the cloud layer within 1500 – 2000 m range exhibit an even stronger elastic backscattering, exceeding 80 $Mm^{-1}sr^{-1}$. However, no significant change of fluorescence backscattering is observed. These results clearly indicate the absence of leaks/contamination of elastic scattering in the fluorescence channel, which in turn allow us monitor fluorescence within cloud layers.

The situation, however, can be different, when the cloud droplets are formed on the aerosol particles, thus fluorescent aerosols are inside the water particles. Fig.5 shows the height – temporal distributions of the lidar signal at 1064 nm and the fluorescence backscattering coefficient on the night 19-20th November 2019.

After 21:50 UTC a thin cloud layer starts to form at the top of the PBL resulting in simultaneous increase of β_F. To quantify the influence of cloud water droplet on the fluorescence backscattering, Fig.6a provides profiles of aerosol and fluorescence backscattering coefficients

https://doi.org/10.5194/amt-2020-291
Preprint. Discussion started: 29 July 2020


Atmospheric Measurement Techniques Discussions

for two temporal intervals 20:00 – 21:30 UTC and 21:30 – 00:30 UTC, prior and after the cloud layer formation respectively. Prior to cloud formation the aerosol load is very low, so backscattering is provided only at 1064 nm and to be distinguished at this figure, the value of β_{1064} is multiplied by factor 100. For 20:00 – 21:30 β_{1064} at 1500 m (height where the cloud forms) is about 0.07 $Mm^{-1}sr^{-1}$. After the cloud formation the backscattering coefficient is shown at 532 nm, because 1064 nm detector in the cloud layer was overloaded. β_{532} increases up to 500 $Mm^{-1}sr^{-1}$ (maximum value) and the fluorescence backscattering increases by approximately factor 5.

Similar scenario occurred on the night 23-24th November 2019 (Fig.6b). Prior to the cloud formation (21:00 – 23:00 UTC) the backscattering coefficient at 900 m height is β_{1064}=0.02 $Mm^{-1}sr^{-1}$ and after cloud formation β_{532} increases up to 130 $Mm^{-1}sr^{-1}$, while β_F again increases about factor 5. The profiles of β_F in Fig.6 prior and after the cloud formations remain the same, below the cloud. It corroborates the suggestion that the cloud was not transported by the air masses with different properties, but the process of water vapor condensation occur, leading to formation of internal mixture of aerosol and cloud particles.

We should recall also, that the enhancement of β_F can not be explained by just insufficient suppression of elastic scattering. The enhancement was observed only inside an aerosol layer, while clouds with similar backscattering coefficients, but outside the aerosol layer, didn't provide the increase of β_{532}. Several possible mechanisms could be responsible for the observed fluorescence backscattering increase. As mentioned above, the fluorescence scattering phase function of microspheres can have a peak in the backward direction (Pan et al., 2002; Veselovskii et al., 2002a). The fluorescence cross section of particles may be subject to hygroscopic effect so impacted by the amount of available water vapor (RH). For example, it is known, that fluorescence cross section of wet bacterial spores is higher than that of dry ones (Kunnil et al., 2004). For insoluble particles, the presence of a water shell can lead also to additional increase of the fluorescence, due to the lens effect produced by the droplet. Similar effect is well known for the soot particles covered by non-absorbing shell (Schnaiter et al., 2005).

One of the objectives of this study was to discuss the possibility to derive the aerosol content within cloud layers, from the fluorescence measurements. Fig.7 shows, for November 15th 2019, 2:45 – 6:15 UTC, the height – temporal distributions of the range corrected lidar signal at 1064 nm and the fluorescence backscattering β_F. Low cloud layers appear at approximately 2000 m and a signal of aerosol fluorescence is observed within this layer up to 3000 m. The vertical profiles of β_{532} and fluorescence backscattering β_F, integrated over this temporal interval, are shown in Fig.8a. Fluorescence backscattering does not change

https://doi.org/10.5194/amt-2020-291
Preprint. Discussion started: 29 July 2020


Atmospheric Measurement Techniques Discussions

significantly inside 1000 – 3500 m height range, thus aerosol content outside and inside the cloud layer is similar. Strong increase of elastic scattering at 2700 m does not lead to significant increase of β_F, hence the mixture of aerosol and cloud particles can be considered as external. Using the results from the previous section for UR aerosol model, the volume density of the ambient particles within the cloud layer can be estimated as ~2 $\mu m^3 cm^{-3}$.

On November 25th 2019 (Fig.8b), a low cloud layer at 850 m leads to increase of β_F by approximately of factor 2, in a similar way as in Fig.6. However, in the cloud above 2000 m, no fluorescence signal, exceeding the noise level, is observed, indicating that the cloud is free of aerosol. Thus, the results in Fig.8 demonstrate, that the fluorescence technique is capable to distinguish between "clean of particles" and "polluted" cloud layers.

Conclusion

In our research we analyzed the feasibility of the fluorescence channel, added to the multiwavelength Mie-Raman lidar for aerosol characterization. The results obtained, demonstrate that the use of an interference filter for selection the part of the fluorescence spectrum allows highly efficient lidar operation. In particular, LILAS lidar with the interference filter of 44 nm width in the fluorescence channel, was able to detect fluorescence signal from weak aerosol layers ($\beta_{1064} < 0.02$ $Mm^{-1}sr^{-1}$) up to 5000 m. During the experiment the fluorescence capacity $G_F = \frac{\beta_F}{\beta_{1064}}$ of aerosol at condition of low RH varied through the $(0.6 – 2.5)\times10^{-4}$ range, being the highest for the smoke and the lowest for the dust particles. The fluorescence capacity depends as well on the relative humidity, because the water uptake at the condition of high RH increases the elastic backscattering, without significant modification of the fluorescence. Thus simultaneous measurements of Mie-Raman and fluorescence lidar open opportunity for the study of the particle hygroscopic growth.

The lidar measurements, in principle, allow to get the quantitative information about the aerosol fluorescence cross section in the elevated aerosol layers. For several atmospheric situations the rough estimations of σ_F were performed in this study and the results obtained look reasonable, comparing with published values for biological particles. Still these results should be taken as preliminary and the next important step in quantification of the fluorescence measurements will be the system calibration, using a lamp with known spectrum. As well, more deep comparison of σ_F obtained from the lidar and laboratory measurements, for different aerosol types, is needed for validation. It should be mentioned, that the fluorescence and multiwavelength Mie-Raman lidar techniques are complimentary. The multiwavelength lidar

https://doi.org/10.5194/amt-2020-291
Preprint. Discussion started: 29 July 2020


Atmospheric Measurement Techniques Discussions

allows aerosol typing and estimation of the particle number and volume densities, that are later used to derive the fluorescence cross sections from observed β_F. The fluorescence measurements, in turn, help to improve the aerosol classification. The synergy of fluorescence and multi-wavelength lidar techniques was not realized in this study, due to too low aerosol loading in November – February period. However, we plan new experiments during Spring – Summer season, when AOD is larger in Lille.

Results presented demonstrate also, that the fluorescence technique can be efficiently used to estimate the particle concentration inside the cloud layer (at least near the cloud base, if penetration depth of the laser radiation is small), which is important in the study of aerosol – cloud interaction. Moreover, our measurements indicate, that aerosol and cloud particles can be mixed both externally and internally. In the clouds formed at the top or inside the aerosol layer (which makes possible internal mixture scenario), significant increase of the fluorescence backscattering coefficient (up to factor 5), was observed. Among possible mechanisms of such enhancement we can assume the increase of fluorescence cross section in solvent state, modification of the scattering phase function of particles embedded in microspheres and the lens effect due to the water shell. At a moment we are not able to specify the mechanism and future studies are needed.

In coming studies we plan additional modifications of the lidar. The efficiency of the fluorescence channel is demonstrated to be high, so the filter bandwidth can be decreased to 10-20 nm, which will make more solid our simplified approach to data analysis. We consider also the possibility to add second fluorescence channel near 550 nm, which should improve selectivity of the fluorescence technique to different aerosol types. The water vapor channel will be returned back to the system, which is essential for the study of particle hygroscopic growth. Collocated measurements of the microwave radiometer of the Laboratoire d'optique atmosphérique will be used to derive the RH profiles. When considering, the aerosol characterization inside the cloud, the possible effect of the multiple scattering on the results will be also analyzed.

Acknowledgments

The authors are very grateful to Service National d'Observation PHOTONS/AERONET-EARLINET from CNRS-INSU, France; to ACTRIS-2 program under the European Union's Horizon 2020 research and innovation programme under grant agreement no. 654109; to Région Hauts-de-France and the Ministère de l'Enseignement Supérieur et de la Recherche (CPER Climibio); and to IDEAS+/ESA Programme for supporting this research.

https://doi.org/10.5194/amt-2020-291
Preprint. Discussion started: 29 July 2020

Atmospheric Measurement Techniques Discussions

Table 1. Parameters of the biomass burning (BB), URban and DUst particles used in the model. The volume $V^{N=1}$ and backscattering coefficient $\beta_{1064}^{N=1}$ are given for a single particle (N=1).

Type	$r_{V,f}$ µm	$r_{V,c}$ µm	σ_f	σ_c	$\frac{C_{V,f}}{C_{V,c}}$	CRI $_{1064}$	$V^{N=1}$ µm^3/cm^3	$\beta_{1064}^{N=1}$ Mm^{-1}sr^{-1}
BB	0.12	3.95	0.4	0.75	1.32	1.51-i.0.02	5.91E-3	1.58E-4
URban	0.175	3.275	0.38	0.75	2.5	1.4-i0.003	1.61E-2	4.69E-4
DUst	0.12	2.32	0.4	0.6	0.05	1.56- i0.001	7.6E-2	2.83E-3

Table.2. The aerosol parameters in elevated layers for three measurement sessions from Fig.3, including the fluorescence β_F and aerosol β_{1064} backscattering coefficients, number N and volume V particle densities, the differential fluorescence cross sections per a single particle $\frac{\sigma_F}{N}$ and per unit volume $\frac{\sigma_F}{V}$, together with spectral density $\frac{\sigma_F}{V\Delta\lambda}$.

Date	Height km	β_F, Mm^{-1}sr^{-1}	β_{1064}, Mm^{-1}sr^{-1}	N, cm^{-3}	V, µm^{3}cm^{-3}	$\frac{\sigma_F}{N}$, 10^{-15} cm^{2}sr^{-1}	$\frac{\sigma_F}{V}$, 10^{-13} cm^{2}sr^{-1}µm^{-3}	$\frac{\sigma_F}{V\Delta\lambda}$, 10^{-15} cm^{2}sr^{-1}µm^{-3}nm^{-1}
30 Nov	4.0	3.0E-6	0.010	63	0.37	0.48	0.81	1.84
16 Jan	5.0	4.88E-6	0.013	82	0.60	0.48	0.81	1.84
6-7 Feb	2.9	5.63E-6	0.096	34	2.58	2.18	0.22	0.5

https://doi.org/10.5194/amt-2020-291
Preprint. Discussion started: 29 July 2020

Atmospheric Measurement Techniques Discussions

435

436 ***References***

437 Alexandrov, M. and Mishchenko, M.: Information content of bistatic lidar observations of
438 aerosols from space, Opt. Expr. 25, 134-150, 2017.
439 Ansmann, A., Riebesell, M., Wandinger, U., Weitkamp, C., Voss, E., Lahmann, W., and
440 Michaelis, W.: Combined Raman elastic-backscatter lidar for vertical profiling of moisture,
441 aerosols extinction, backscatter, and lidar ratio, Appl.Phys.B, *55*, 18-28, 1992.
442 Burris, J., McGee, T.J., Heaps, W.: UV Raman cross sections in nitrogen, Appl. Spectroscopy
443 46, 1076, 1992.
444 Burton, S. P., Ferrare, R. A., Hostetler, C. A., Hair, J. W., Rogers, R. R., Obland, M. D., Butler,
445 C. F., Cook, A. L., Harper, D. B., and Froyd, K. D.: Aerosol Classification of Airborne High
446 Spectral Resolution Lidar Measurements – Methodology and Examples, Atmos. Meas. Tech.,
447 5, 73–98, doi:10.5194/amt-5-73-2012, 2012.
448 Burton, S. P., Chemyakin, E., Liu, X., Knobelspiesse, K., Stamnes, S., Sawamura, P., Moore, R.
449 H., Hostetler, C. A., and Ferrare, R. A.: Information content and sensitivity of the 3β+2α
450 lidar measurement system for aerosol microphysical retrievals, Atmos.Meas. Tech., 9, 5555–
451 5574, 2016.
452 Dubovik, O., Holben, B., Eck, T.F., Smirnov, A., Kaufman, Y.J., King, M.D., Tanre, D.,
453 Slutsker, I.: Variability of absorption and optical properties of key aerosol types observed in
454 worldwide locations, J. Atmos. Sci., 59, 590–608, 2002.
455 Dubovik, O., Sinyuk, A., Lapyonok, T., Holben, B.N., Mishchenko, M., Yang, P., Eck, T.F.,
456 Volten, H., Munoz, O., Veihelmann, B., van der Zande, W.J., Leon, J.-F., Sorokin, M.,
457 Slutsker, I.: Application of spheroid models to account for aerosol particle nonsphericity in
458 remote sensing of desert dust, *J. Geophys. Res.*, 111, D11208, doi:10.1029/2005JD006619,
459 2006.
460 Hill, S. C., Williamson, C. C., Doughty, D. C, Pan, Y.-L., Santarpia, J. L., Hill, H. H.: Size-
461 dependent fluorescence of bioaerosols: Mathematical model using fluorescing and absorbing
462 molecules in bacteria, J. Quant. Spectr. Radiat. Trans., 157, 54–70, 2015.
463 Horvath, H., Gunter, R. L., and Wilkison, S. W.: Determination of the coarse mode of the
464 atmospheric aerosol using data from a forward-scattering spectrometer probe, Aerosol
465 Sci. Technol., 12, 964–980, 1990.
466 Hu, Q., Goloub, P., Veselovskii, I., Bravo-Aranda, J.-A., Popovici, I., Podvin, T., Haeffelin, M.,
467 Lopatin, A. , Dubovik, O., Pietras, C., Huang, X., Torres, B., and Chen, C.: Long-range-
468 transported Canadian smoke plumes in the lower stratosphere over northern France, Atmos.
469 Chem. Phys. 19, 1173 – 1193, 2019. doi.org/10.5194/acp-19-1173-2019.

https://doi.org/10.5194/amt-2020-291
Preprint. Discussion started: 29 July 2020

Atmospheric Measurement Techniques Discussions

470 Huffman, J.A., Perring, A.E., Savage, N.J., Clot, B., Crouzy, B., Tummon, F., Shoshanim, O.,
471 Damit, B., Schneider, J., Sivaprakasam, V., Zawadowicz, M.A., Crawford, I., Gallagher, M.,
472 Topping, D., Doughty, D.C., Hill, S.C., Pan, Y.: Real-time sensing of bioaerosols: Review
473 and current perspectives, Aerosol Science and Technology, 2019. DOI:
474 10.1080/02786826.2019.1664724
475 Immler, F., Engelbart, D., Schrems, O.: Fluorescence from atmospheric aerosol detected by a
476 lidar indicates biogenic particles in the lower stratosphere, Atmos. Chem. Phys. 5, 345–355,
477 2005.
478 Kerker, M., and Druger, S. D.: Raman and fluorescent scattering by molecules embedded in
479 spheres with radii up to several multiples of the wavelength, Appl. Opt. 18**,** 1172–1179,
480 1979.
481 Klett J.D., "Lidar inversion with variable backscatter/extinction ratios", Appl.Opt. 24, 1638-
482 1643, 1985.
483 Kunnil, J., Swartz, B., Reinisch, L.: Changes in the luminescence between dried and wet bacillus
484 spores, Appl. Opt. 43, 5404 – 5409, 2004.
485 Li, B., Chen, S., Zhang, Y., Chen, H., Guo, P.: Fluorescent aerosol observation in the lower
486 atmosphere with an integrated fluorescence-Mie lidar, J. Quant. Spectr. Rad. Transf., 227,
487 211–218, 2019.
488 Miyakawa, T., Kanaya, Y., Taketani, F., Tabaru, M., Sugimoto, N., Ozawa, Y., and Takegawa,
489 N.: Ground-based measurement of fluorescent aerosol particles in Tokyo in the spring of
490 2013: potential impacts of nonbiological materials on autofluorescence measurements of
491 airborne particles, J. Geophys. Res. Atmos., 120, 1171–1185, 2015,
492 doi:10.1002/2014JD022189.
493 Müller, D., Wandinger, U., and Ansmann, A.: Microphysical particle parameters from extinction
494 and backscatter lidar data by inversion with regularization: theory, Appl. Opt. 38, 2346-2357,
495 1999.
496 Pan, Y.L., Hill, S.C., Wolf, J.P., Holler, S., Chang, R.K., Bottiger, J.R.: Backward-enhanced
497 fluorescence from clusters of microspheres and particles of tryptophan, Appl. Opt. 41, 2994-
498 2999, 2002.
499 Pan, Y.-L., Pinnick, R.G., Hill, S.C., Rosen, J.M., and Chang, R.K.: Single-particle laser-
500 induced-fluorescence spectra of biological and other organic-carbon aerosols in the
501 atmosphere: Measurements at New Haven, Connecticut, and Las Cruces, New Mexico, J.
502 Geophys. Res., 112, D24S19, doi:10.1029/2007JD008741, 2007.
503 Pan, Y.-L.: Detection and characterization of biological and other organic-carbon aerosol
504 particles in atmosphere using fluorescence, J. Quant. Spectr. Radiat. Trans. 150, 12–35, 2015

https://doi.org/10.5194/amt-2020-291
Preprint. Discussion started: 29 July 2020


Atmospheric Measurement Techniques Discussions

505 Rao, Z., He, T., Hua D, Wang, Y., Wang, X., Chen, Y., Le J.: Preliminary measurements of
506 fluorescent aerosol number concentrations using a laser-induced fluorescence lidar, Appl.
507 Opt. 57, 7211-7215, 2018.
508 Reichardt, J.: Cloud and aerosol spectroscopy with Raman lidar, J. Atm. Ocean. Tech., 31,
509 1946-1963, 2014.
510 Reichardt, J., Leinweber, R., Schwebe, A.: Fluorescing aerosols and clouds: investigations of co-
511 existence, Proceedings of the 28th ILRC, Bucharest, Romania, 25-30 June, 2017.
512 Saito, Y., Ichihara, K., Morishita, K., Uchiyama, K., Kobayashi, F., Tomida, T.: Remote
513 detection of the fluorescence spectrum of natural pollens floating in the atmosphere using a
514 laser-induced-fluorescence spectrum (LIFS) lidar, Remote Sens., 10, 1533, 2018.
515 doi:10.3390/rs10101533.
516 Schnaiter, M., Linke, C., Mohler, O., Naumann, K. H., Saathoff, H., Wagner, R., Schurath, U.,
517 and Wehner, B.: Absorption amplification of black carbon internally mixed with secondary
518 organic aerosol, J. Geophys. Res., 110, D19204, 2005.
519 Sugimoto, N., Huang, Z., Nishizawa, T., Matsui, I., Tatarov, B.: Fluorescence from atmospheric
520 aerosols observed with a multichannel lidar spectrometer," Opt. Expr. 20, 20800-20807,
521 2012.
522 Venable, D. D., Whiteman, D. N., Calhoun, M. N., Dirisu, A.O., Connell, R. M., Landulfo, E.:
523 Lamp mapping technique for independent determination of the water vapor mixing ratio
524 calibration factor for a Raman lidar system, Appl. Opt., 50, 4622 - 4632, 2011.
525 Veselovskii, I., Griaznov, V., Kolgotin, A., Whiteman, D.: "Angle- and size-dependent
526 characteristics of incoherent Raman and fluorescent scattering by microsoheres 2.: Numerical
527 simulation", Appl. Opt. 41, 5783-5791, 2002a.
528 Veselovskii I., Kolgotin, A., Griaznov, V., Müller, D., Wandinger, U., Whiteman, D.: Inversion
529 with regularization for the retrieval of tropospheric aerosol parameters from multi-
530 wavelength lidar sounding, Appl.Opt. 41, 3685-3699, 2002b.
531 Veselovskii, I., Goloub, P., Hu, Q., Podvin, T., Whiteman, D. N., Korenskiy, M., Landulfo, E.:
532 Profiling of CH4 background mixing ratio in the lower troposphere with Raman lidar: a
533 feasibility experiment., Atmos. Meas. Tech. 12, 119–128, 2019. doi.org/10.5194/amt-12-
534 119-2019.
535 Whiteman, D. N., B. Demoz, P. Di Girolamo, J. Comer, I. Veselovskii, K. Evans, Z. Wang, M.
536 Cadirola, K. Rush, G. Schwemmer, B. Gentry, S. H. Melfi, B. Mielke, D. Venable, T. Van
537 Hove, "Raman Water Vapor Lidar Measurements During the International H2O Project. I.
538 Instrumentation and Analysis Techniques", J. Atmos. Oceanic Technol., 23, 157-169, 2006.
539

https://doi.org/10.5194/amt-2020-291
Preprint. Discussion started: 29 July 2020

Atmospheric Measurement Techniques Discussions

Figures

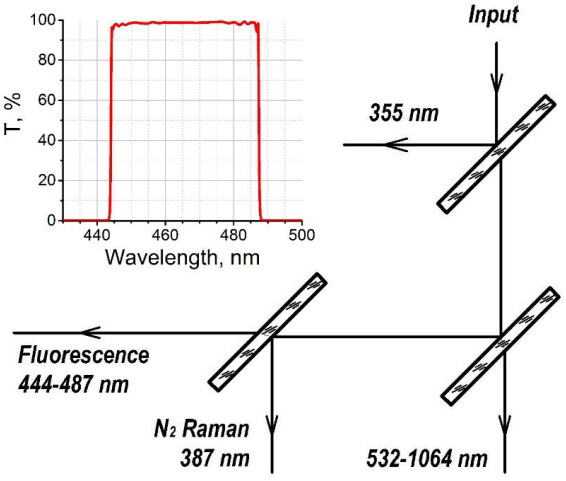

Fig.1 Optical scheme of the elastic, Raman and fluorescence backscatters separation together with transmission curve of the interference filter in the fluorescence channel.

https://doi.org/10.5194/amt-2020-291
Preprint. Discussion started: 29 July 2020

Atmospheric Measurement Techniques Discussions

551

552
553
554

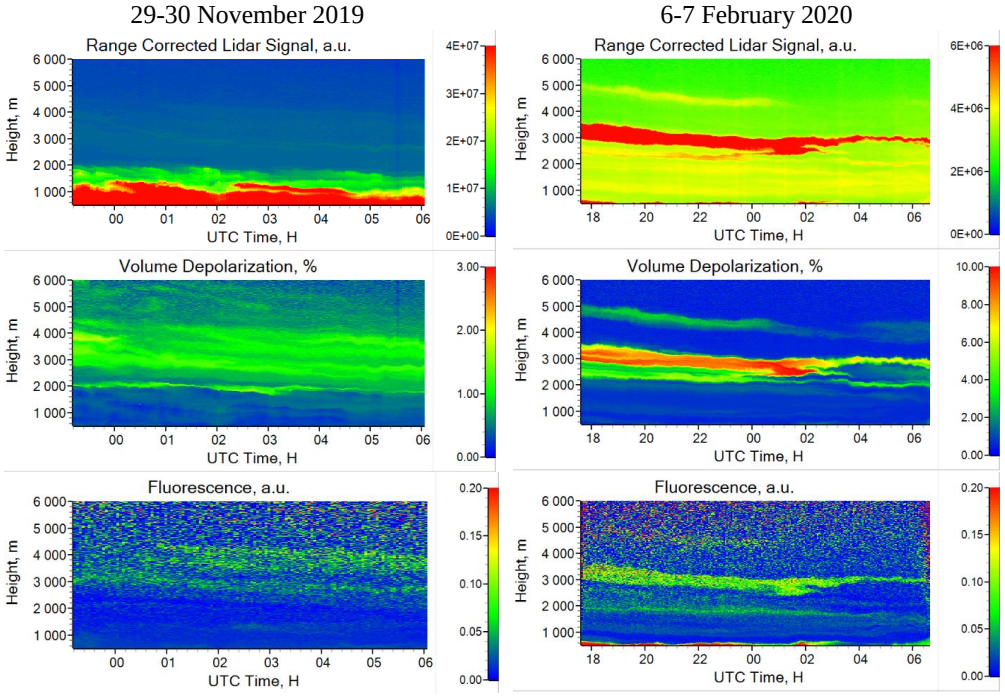

555 Fig.2. The range corrected lidar signal at 1064 nm, volume depolarization ratio δ_{1064} and
556 fluorescence backscattering measured at Lille, on 29-30 November 2019 (on the left) and 6-7
557 February 2020 (on the right).
558
559

https://doi.org/10.5194/amt-2020-291
Preprint. Discussion started: 29 July 2020

Atmospheric Measurement Techniques Discussions

560

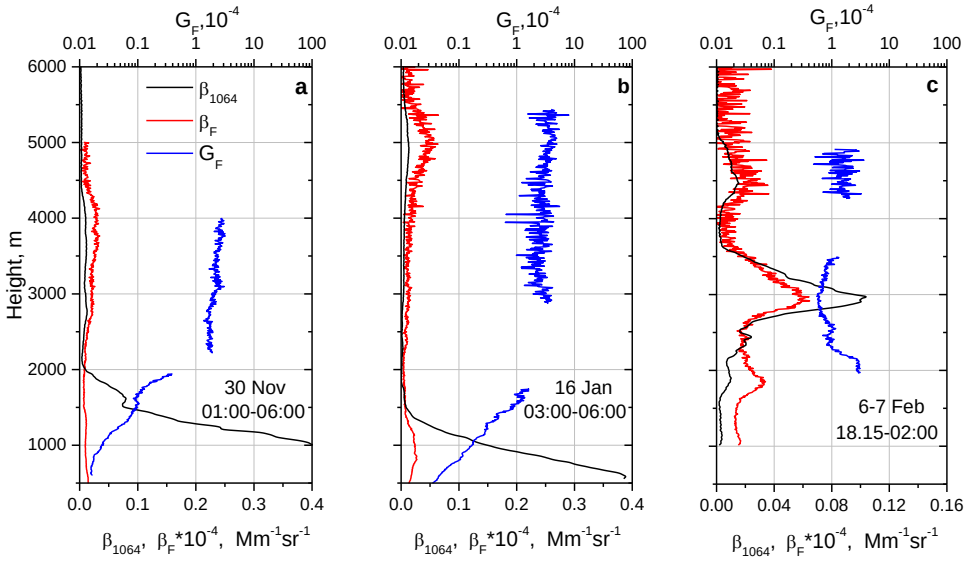

561 Fig.3 Vertical profiles of aerosol (β_{1064}) and fluorescence (β_F) backscattering coefficients
562 together with the fluorescence capacity (G_F) on (a) 30 November 2019, (b) 16 January 2020 and
563 (c) 6-7 February 2020.

564

565

566

567

568

https://doi.org/10.5194/amt-2020-291
Preprint. Discussion started: 29 July 2020

Atmospheric Measurement Techniques Discussions

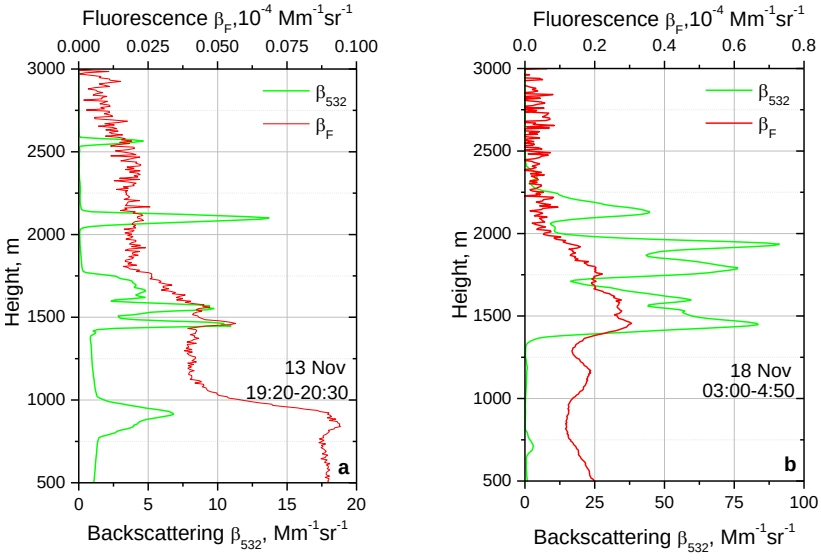

569 Fig.4. Aerosol (β_{532}) and fluorescence (β_F) backscattering coefficients on 13 and 18 November
570 2019.

571

572

573

https://doi.org/10.5194/amt-2020-291
Preprint. Discussion started: 29 July 2020

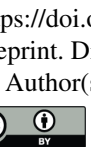

Atmospheric Measurement Techniques Discussions

574

575

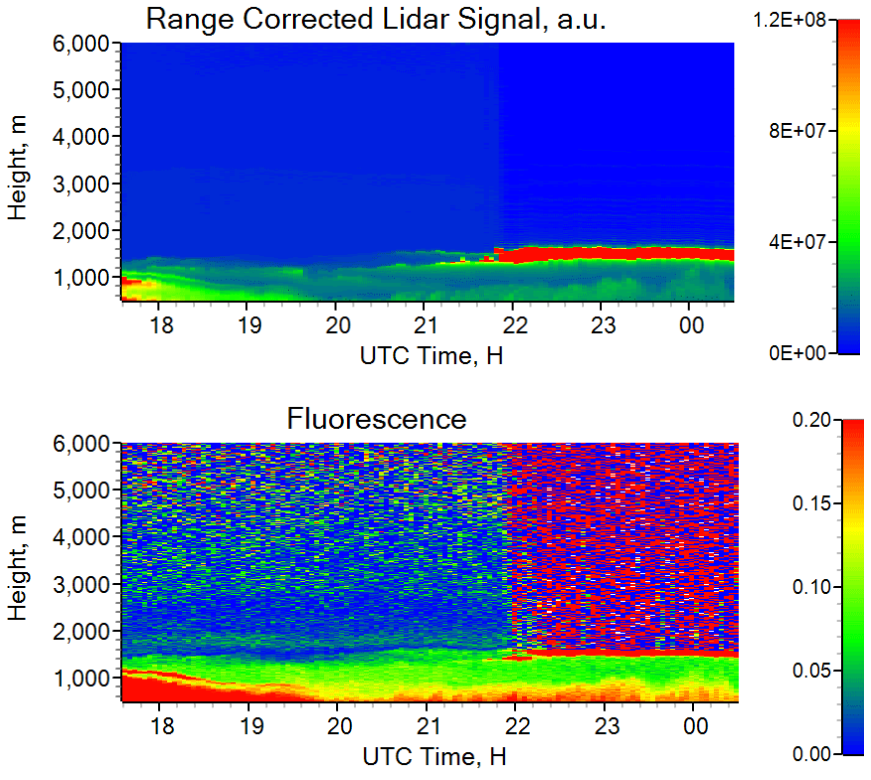

576

577

578

579 Fig.5. Height-temporal distribution of the range corrected lidar signal at 1064 nm and
580 fluorescence backscattering coefficient β_F (in arbitrary units) on 19-20 November 2019.

https://doi.org/10.5194/amt-2020-291
Preprint. Discussion started: 29 July 2020

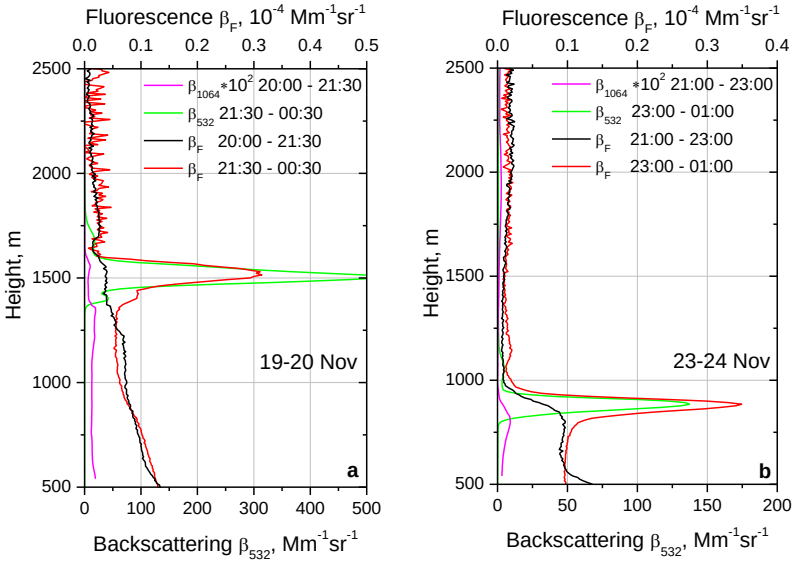

581 Fig.6. Aerosol and fluorescence backscattering coefficients on (a) 19-20 and (b) 23-24
582 November 2019 for two time intervals: prior and after cloud formation. Backscattering
583 coefficient β_{1064} prior to cloud formation is low, so it is multiplied by factor 100 to be
584 distinguished at this figure.
585
586

https://doi.org/10.5194/amt-2020-291
Preprint. Discussion started: 29 July 2020

Atmospheric Measurement Techniques Discussions

587

588

589

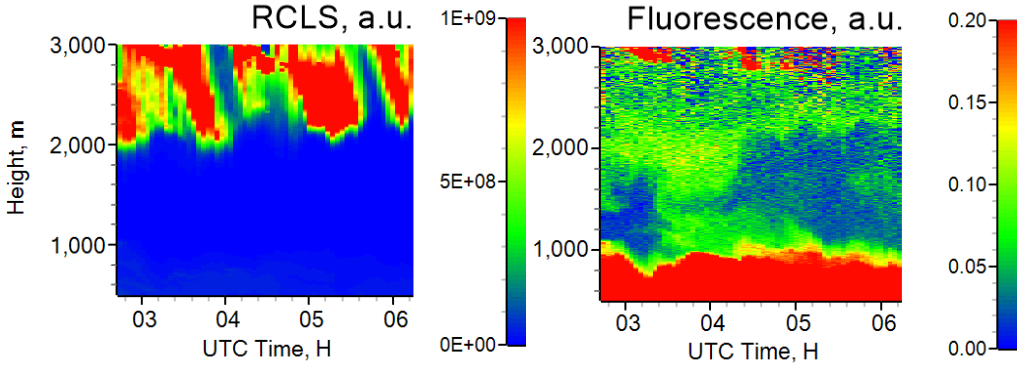

590

591 Fig.7. Height-temporal distribution of the range corrected lidar signal (RCLS) at 1064 nm and

592 the fluorescence backscattering coefficient on 15 November 2019.

593

https://doi.org/10.5194/amt-2020-291
Preprint. Discussion started: 29 July 2020

Atmospheric Measurement Techniques Discussions

594

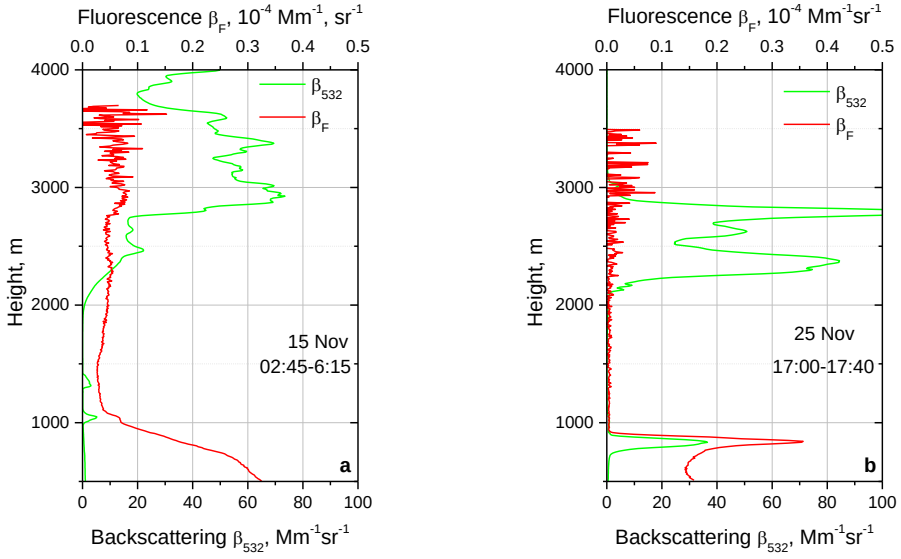

595 Fig.8. Aerosol (β_{532}) and fluorescence (β_F) backscattering coefficients on (a) 15 and (b) 25
596 November 2019.

597